Available online at www.sciencerepository.org

Science Repository

Research Article

Imaging Performance of a Multimodal Module to Enhance Preclinical Irradiator Capabilities

Joël Daouk, Justine Jubréaux, Alicia Chateau, Hervé Schohn and Sophie Pinel*

CRAN, BioSiS Department, UMR Université de Lorraine-CNRS 7039, Nancy, France

ARTICLE INFO

Article history:
Received: 21 January, 2020
Accepted: 8 February, 2020
Published: 28 February, 2020

Keywords:
Preclinical radiotherapy
X-ray imaging
Bioluminescence
image-guided radiotherapy

ABSTRACT

This article highlights the performance measurements of an optical device which aims at upgrading pre-clinical irradiators. The evaluated device allows acquiring X-ray as well as bioluminescence images with a single sensor. The latter consists of a supercooled camera equipped with a 1024x1024 charge coupling device (each element measuring 13x13µm²). X-ray imaging is feasible, thanks to a conversion phosphor screen. Phantom acquisitions revealed a spatial resolution of 2.5 line pairs per millimetre (0.2mm) for X-ray imaging and between 0.4 and 0.7mm for bioluminescence images. Image homogeneity was 0.8 for radiographic images with preclinical imaging parameters and higher than 0.9 for optical images. For functional imaging, contrast to noise ratio (CNR) ranged from 1.3 (for contrast of 2:1 and 0.1s acquisition) up to 253 (for contrast of 32:1 and 5s acquisition). CNR was related to acquisition duration. The device's overall performance revealed that it is suitable to upgrade existing irradiators and improve laboratory capabilities toward image-guided radiotherapy.

Introduction

Molecular imaging offers many unique opportunities to study biological processes in intact organisms. Bioluminescence imaging (BLI) is most frequently used for tracking cancer cells and studying their distribution and activity in vivo. BLI is ideally suited to image fundamental biological processes in vivo due to the fact that it is easy to use, cost-effective, very sensitive, has a high signal-to-noise ratio, low background, and short acquisition time [1, 2]. BLI signal relies on the degradation of luciferin by luciferase enzyme via oxidation/decarboxylation reactions and formation of an intermediate excited state that releases photons to return to stability. Bioluminescence can be detected as deep as a few centimeters within the tissue, which allows in situ imaging without any specific observation device (such as glass window), and then orthotopic cell implantation can be observed [3]. BLI is a simple imaging technique (albeit requiring cell lines expressing luciferase enzyme). It can be used to follow disease progression or treatment efficacy by reducing the number of animals requiring by the experiment as it allows several measurements of the biological activity in a single animal.

Technically speaking, BLI photons (emitted broadly around 560 nm) are detected by highly sensitive charge-coupled devices (CCD). The CCD is usually supercooled to around -90 ◦C to reduce thermal noise, thereby increasing its ability to detect very low levels of signal. Such technology has been proven to be consistent and reproducible with ±8% standard deviation around mean values of the same acquired object [4]. However, BLI presents some well-known pitfalls. Firstly, the efficiency of bioluminescent light transmission through an animal from its origin depends largely on the type and depth of overlying tissue as well as its scattering properties. In addition, hemoglobin absorbs light, leading to signal underestimation for highly vascularized organs compared to skin or muscle. Secondly, BLI traditionally has provided relatively poor spatial resolution due to scattering and diffraction of light through tissue. That makes localization of the signal source inaccurate [5]. Moreover, as cells do not emit any signal if they do not express luciferase enzyme, BLI does not provide any anatomical information to localize tagged cells. Then, the addition of a morphological modality, such as X-ray imaging, is of significant interest to provide information additional to BLI images. Manufacturers now offer hybrid systems that allow bioluminescence and/or X-ray imaging. In this work, we characterize the imaging performance of a multimodal image device based on a cooled

*Correspondence to: Sophie Pinel, CRAN, BioSIS Department, UMR Université de Lorraine, CNRS 7039, Faculté de médecine, Bât. D, 9 avenue de la forêt de Haye, Nancy, France; E-mail: sophie.pinel@univ-lorraine.fr

http://dx.doi.org/10.31487/j.COR.2020.02.01

optical camera. That can be used to upgrade an existing preclinical irradiator toward molecular/anatomical imaging, a mandatory step toward image-guided radiotherapy.

Materials and Methods

I OptiMAX Device

The OptiMAX (Precision X-Ray Inc, North Brandford, CT) consisted of a cooled monochrome CCD camera supercooled down to -80°C. The sensor matrix size was 1024x1024 pixels, each pixel measuring 0.013x0.013 mm. A filter wheel was placed just in front of the camera focal lens to hold user-defined filters for optical imaging. To avoid direct X-ray irradiation when using the irradiator without imaging, the camera was deported in a shielded compartment and a mirror guided photons from the imaging chamber to the CCD (Figure 1).

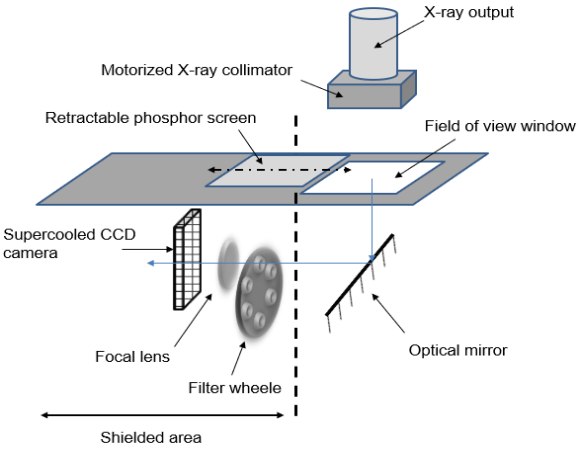

Figure 1: OptiMAX principle drawing. The CCD camera is positioned with its focal lens and filter wheele in a shielded area, inside the X-RAD 320 irradiation chamber, to protected materials from X-rays. X-rays are delivered throughout a motorized collimator and interact with a retractable phosphor screen for radiographic images. Photons are then converted into visible photons which are reflected onto the mirror and recorded by the CCD sensor. Bioluminescence is performed in the same way with the film out of the field of view as it provides visible photons directly.

II Radiographic Performance

Radiographs are performed via a phosphor screen, which is automatically positioned in front of the main glass of the device. Image quality was performed with a TOR18FG phantom (Leeds Test Objects Ltd, Roecliffe, UK). This phantom allows measurement of image quality by monitoring brightness and contrast levels, determining the resolution limit (between 0.5 and 5 line pairs per millimeter – lp mm^{-1}), and by finding the low-contrast sensitivity. There are 18 details/circles of 8 mm diameter with a contrast range of 0.9% to 16.7% at 70 kV using 1 mm of Copper on top of the phantom.

i Spatial Resolution

The theoretical resolution of the sensor, also referred to as the image space resolution for the system, was calculated by multiplying the pixel size in µm by 2 (to create a pair), and dividing that into 1000 to convert to mm. Considering OptiMAX FOV and sensor matrix size, the ideal spatial resolution limit was 2.56 lp mm^{-1}. We set the tube parameters to 40 kV, 5mA and 5s exposure, as recommended by the manufacturer. Camera focus was set to 0.02, and aperture was set to 0.95, meaning that the phantom was placed just in front of the main glass and that we limited the camera aperture. Profiles were drawn across each resolution test pattern subset. The smallest resolved subset was considered as the effective spatial resolution of the device for X-ray imaging.

ii Signal to Noise Ratio and Homogeneity

Ten circular regions of interest (ROI) of 7 mm diameter were manually defined on the phantom background. We measured the minimum, maximum values as well as the mean and the standard deviation of each ROI. Signal to noise ratio (SNR) was defined as

$$\mathrm{SNR} = \frac{\overline{\mathrm{mean}_{\mathrm{ROI}}}}{\overline{\sigma_{\mathrm{ROI}}}}$$

and homogeneity was defined as

$$\mathrm{homogeneity} = 1 - \frac{\mathrm{max}_{\mathrm{allROIs}} - \mathrm{min}_{\mathrm{allROIs}}}{\mathrm{max}_{\mathrm{allROIs}} + \mathrm{min}_{\mathrm{allROIs}}}$$

SNR and homogeneity were measured on images acquired at 40 kV, 70 kV and 110 kV (the latter two with addition of a 1-mm copper plate).

iii Contrast

The contrast was assessed with the phantom low-contrast objects. The last observed object detected at 40 kV (without copper plate), and 70 kV and 110 kV (with 1-mm copper) defined the contrast limits for these acquisition conditions. For all X-ray studies, no filter was applied to images prior to analysis.

III Physical Assessment of Luminescence Performance

i Spatial Resolution

A phosphorescent paint was used to mimic bioluminescence emission (Signals™, Perigny, France). A 30 G needle (outer diameter = 0.254mm) was used to create a point source, paint was aspirated into the needle and the outer edge were carefully cleaned to remove unwanted signal. The needle was placed vertically 5 mm above the OptiMAX glass. Images were acquired with the following parameter: binning = 1, focus = 0.1, aperture = 0.9 and acquisition time = 1s. No filter was applied to images prior to analysis. Profiles were drawn across the point source image in X and Y direction to assess both X and Y spatial resolution, and full width at half maximum was computed to deduce to actual system spatial resolution. The point source has been acquired six more times at various places in the FOV.

ii Contrast

The paint was diluted with dimethylbenzene to obtain contrasts from 1 to 1/32 concentration. Paint samples were placed into a 96-well plate (3 wells per concentration) and acquisitions were acquired with the same parameters as the spatial resolution assessment. ROI was defined to cover 90% of each well surface, and the mean intensity, as well as the standard deviation and the minimum/maximum were extracted. Contrast

recovery (CR) was computed to assess the system's ability to accurately display contrasts and is defined as:

$$CR_t = \frac{\overline{S_t} - \overline{S_{lowest}}}{\overline{S_{lowest}}}$$

where $\overline{S_t}$ is the mean signal in the concerned well t and $\overline{S_{lowest}}$ is the mean signal in the well where the paint was the most diluted. Moreover, we computed the contrast to noise ratio (CNR) to estimate the detectability of bioluminescent foci in the images. CNR was defined as follows:

$$CNR_t = \frac{\overline{S_t} - \overline{S_{lowest}}}{\sigma_{lowest}}$$

where s_{lowest} is the signal standard deviation in the lowest contrast wells. We also assessed luminescent homogeneity by defining ROIs onto the 3 lowest contrast plates. Homogeneity was then defined as

$$\text{homogeneity} = 1 - \frac{\max_{allROIs} - \min_{allROIs}}{\max_{allROIs} + \min_{allROIs}}$$

IV Biological Assessment

i Cell Culture

U87-Luc2 malignant glioma cell was purchased from the American Type Culture Collection (ATCC, Manassas, VA, US). According to the manufacture recommendations, cells were cultivated in DMEM medium (ATCC, Manassas, VA, US) supplemented with 10% heat-inactivated fetal bovine serum (Sigma Aldrich, Saint-Louis, MO, US), 1% penicillin/streptomycin (Sigma Aldrich, Saint-Louis, MO, US) and 8 µg/mL blasticin (Fischer scientific, Hampton, NH, US) to maintain a Luc2 positive selective pressure on cell. Two renewals of medium were performed each week, and the cells were harvested by trypsinization. To assess the system sensitivity, experiments were performed with different U87-Luc2 and D-luciferin concentrations. Cells were placed in Eppendorf tubes from 2000 to 200,000 cells per tube. Each tube was exposed to D-luciferin at various concentrations form 20 µg/mL to 150 µg/mL, the latter being recommended by the supplier. The tubes were centrifuged for 7 min at 170 g, and the pellets were placed in the OptiMAX system. Imaging parameters were the same as for the phantom acquisitions with an acquisition time of 90 sec as the bioluminescent signal is obviously lower than the luminescent paint. The images were analyzed with ImageJ software.

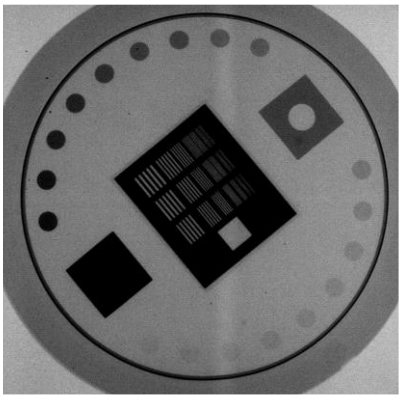

Figure 2: TOR18FG phantom radiographic image. Image was acquired at 40 kV, 5mA without copper plate. These parameters are those recommended by the manufacturer for *in vivo* imaging.

Results and Discussion

Radiographic image of the TOR18FG phantom, acquired in preclinical conditions, is presented in (Figure 2). We were able to discriminate all line pairs up to 2.5 lp mm^{-1}. Obtained profiles are presented in (Figure 3). It is noteworthy that several preclinical imagers providing CT images yielded spatial resolution from 1.15 to 1.82 lp mm^{-1} [6]. We obtained SNR of 32.3, 36 and 46.1 for 40 kV, 70 kV and 110 kV respectively. Homogeneity was good for 40 kV images (0.80) and improved for 70 and 110 kV images (0.88 and 0.89 respectively). As observed in (Figure 2), all contrast objects were visible at 40 kV without copper. When acquiring image at 70 kV and 110 kV with 1-mm copper, the contrast limit was 3.2% and 2.2%, respectively. The main system limitation for X-ray or γ imaging is the phosphor screen used to convert high energy photons to visible ones recorded by the camera. Indeed, if the delivered photons energy is too high, the number of visible photons will be too high, and the conversion screen will be saturated, yielding the blinding of the CCD sensor.

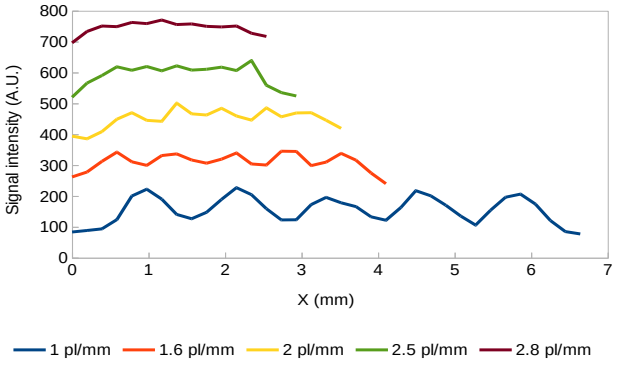

Figure 3: Profiles obtained for spatial resolution patterns on TOR18FG@40kV image. 5 peaks were observed from 1 to 2.5 pairs of lines per millimeters.

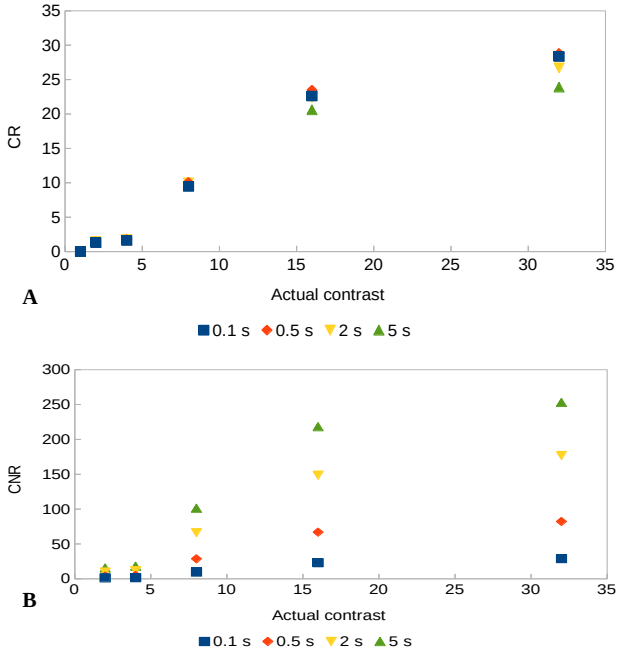

Figure 4: Contrast recovery – CR – (**A**) and contrast-to-noise ratio – CNR – (**B**) obtained on luminescence images.

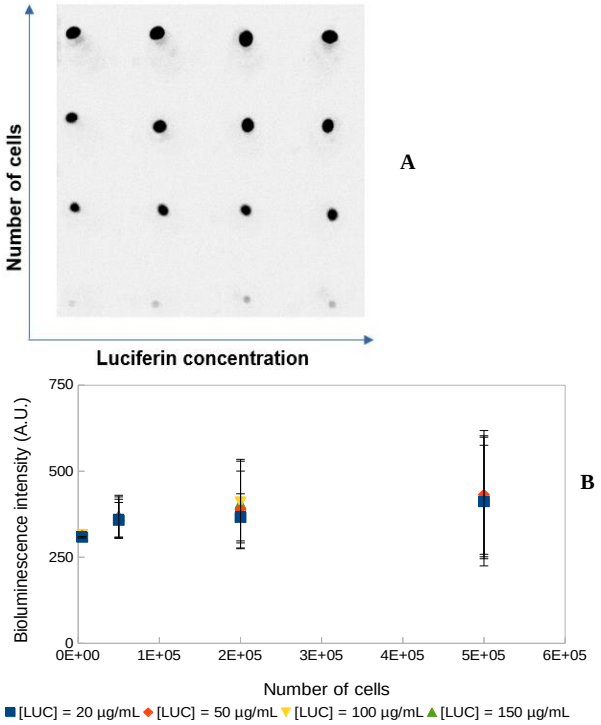

Figure 5: Biolmuninescence image obtained with U87-Luc2 cells exposed to increasing luciferin concentration (**A**). Signal intensity was independent to luciferin concentration but increased with the number of cells in the pellet (**B**).

For the bioluminescence images, the spatial resolution has been measured at 0.39 ± 0.28 mm in the X direction and 0.68 ± 0.6 mm in the Y direction. SNR and homogeneity were inversely related to acquisition duration. SNR varied from 198.4±2.9 down to 49.44±2.19 for acquisitions from 0.1s to 5s respectively. In the same way, homogeneity varied from 0.985 ± 0.001 to 0.941 ± 0.002 for acquisitions from 0.1s to 5s respectively. Contrast recovery and contrast-to-noise ratio studies are depicted in (Figure 4). CR was underestimated for contrast lower than 5 (respectively 1.4 and 1.7 in average for contrasts of 2 and 4 without taking acquisition time into consideration). Then, the contrasts were overestimated (9.8 and 22.3 for contrasts of 8 and 16 respectively). For the highest contrast, we observed a kind of saturation: CR = 26.9 for an actual contrast of 32. This can be attributed to a saturation phenomenon due to the high luminescence produced by the paint at high concentrations. In addition, CR did not depend on the acquisition time except for the longest acquisition and the higher contrast. CNR was directly related to acquisition duration. Whatever the acquisition duration, CNR was high for contrast of 8 and more. The 2D cell image is presented in (Figure 5). We have been able to observe all wells, even the ones with the lowest cells and luciferin concentrations, highlighting the high sensor sensitivity. We observed that signal intensity increased with the number of cells, as expected. However, it was independent of the luciferin concentration.

Conclusion

The assessed device demonstrated robust imaging characteristics. Indeed, both modalities (X/γ and bioluminescence) provided very low noise in images combined with infra millimetric spatial resolution, which is suitable for preclinical imaging. The bioluminescence images also showed high uptakes detectability associated and good contrast restitution. Upgrading an existing irradiator with such a multimodal imaging device is a reasonable investment in laboratories willing to optimize their preclinical studies.

Acknowledgments

This work was funded by the CPER Lorraine 2015-2020 IT2M-IMTI program.

REFERENCES

1. O'Neill K, Lyons SK, Gallagher WM, Curran KM, Byrne AT (2010) Bioluminescent imaging: a critical tool in pre-clinical oncology research. *J Pathol* 220: 317-327. [Crossref]
2. Xu T, Close D, Handagama W, Marr E, Sayler G et al. (2016) The Expanding Toolbox of In Vivo Bioluminescent Imaging. *Front Oncol* 6: 150. [Crossref]
3. Sadikot RT, Blackwell TS (2005) Bioluminescence imaging. *Proc Am Thorac Soc* 2: 537-540, 511-2. [Crossref]
4. Wu JC, Sundaresan G, Iyer M, Gambhir SS (2001) Noninvasive optical imaging of firefly luciferase reporter gene expression in skeletal muscles of living mice. *Mol Ther* 4: 297-306. [Crossref]
5. van der Horst G, Buijs JT, van der Pluijm G (2015) Pre-clinical molecular imaging of "the seed and the soil" in bone metastasis. *Bone Cancer* Ch. 46, 557-570.
6. Johnstone CD, Lindsay P, Graves EE, Wong E, Perez JR et al. (2017) Multi-institutional MicroCT image comparison of image-guided small animal irradiators. *Phys Med Biol* 62: 5760-5776. [Crossref]